ingegneria sismica
International Journal of Earthquake Engineering
Anno XLIII - Num. 3 - 2026

Optimizing Desalination Processes for Marble Artifacts: A Study on Compound Modifiers and Salt Extraction Efficiency

Fengsheng Wang[1], *Yukuan Wang*[1] *and Hongli Liu*[1,*]

[1] Colloge of Cultural Heritage, Beijing City University, Shunyi, Beijing, 101309, China

SUMMARY: *A relatively large number of marble cultural relics, such as railings, have been preserved at BeiYue Temple. Because they are old, have been exposed to salt for a long time, and have not been preserved properly, these objects are now damaged by salt weathering. To mitigate salt damage, two typical base materials were selected for research on the effect of desalination treatment in this study: desalination pulp and rice paper. Three sets of compound additives at different ratios (1:2, 1:2.5 and 1:3) were added to these materials and then desalinated. At the same time, many other ways were employed to evaluate the desalinisation effect and changes in the marble surface, such as ion chromatography, X-ray diffraction (XRD), X-ray fluorescence (XRF) spectroscopy, conductivity measurement and digital microscopy. Based on the above results, the 1:2 polyacrylic acid-Poly(epoxysuccinic acid) (PAA-PESA) formulation showed the highest conductivity value (244 μS/cm) and was thus most effective for salt removal; as a result, visibly cleaner macro- and micro-surfaces were obtained after treatment. On the other hand, the 1:2.5 and 1:3 ratios were still relatively large and small black particulate contaminants. Compound modifiers were also added to increase the yield of soluble salts for the experimental group over that in the control group. Increase the supersaturation of the salt solution to improve desalination; thus, increase the extent of dissolution and salt removal. The above results provide some assistance for the research on desalination methods of marble conservation and offer a scientific basis for the preservation of salt-affected stone artifacts.*

KEYWORDS: *Stone Cultural Relics; Marble; Desalination; Salt-Extraction Pulp; Cultural Heritage Preservation*

1 Introduction

Salt crystallization inside porous materials is a reason for the structural damage of buildings in all weather [1-4]. Salt weathering [5] is a cause of damage to the structure of stone and thus leads to all kinds of rock degradation in all sorts of environments. Soluble salts [6, 7] are known to reduce the durability of stone and are a main cause of surface powdering, delamination and spalling in cultural stone relics [8]. The main ions of salt in soil and groundwater are sulfate (SO_4^{2-}), chloride (Cl^-), nitrate (NO_3^-), and carbonate (CO_3^{2-}). These salts are absorbed by the stone through capillarity and then recrystallise repeatedly. When soluble salts crystallize inside the micropores of rocks [9], the resulting stress will cause the formation of microcracks and damage [10]. In a dry and hot climate, an over-saturated solution [11] will evaporate, leading to salt precipitation on the outside of the relics. At the same time, in a warm and humid climate, salts will be dissolved and transported into the pores of the rock; if water in those pores then

*lhl6006@126.com
https://doi.org/10.65102/is20261142
Published: 10 June, 2026

freezes, it can cause expansion and damage. This continuous cycle of "migration and infiltration [12-14]", "crystallization and expansion [15, 16]", and "moisture dissolution [17]" accelerates the development of efflorescence and powdering [18]. Sodium chloride (NaCl) is a type of deterioration that is relatively widespread among various salt-related damage processes to stone cultural relics. At the same time, the decomposition of sodium sulfate (Na_2SO_4) may also cause a phase change and thus serious structural damage. Through repeated dissolution and recrystallisation [19, 20], Na_2SO_4 is converted into a highly unstable crystalline phase, such as the metastable heptahydrate phase ($Na_2SO_4 \cdot 7H_2O$) [21]. With multiple cycles, the metastable phase is finally converted into the less soluble and more stable thenardite phase ($Na_2SO_4 \cdot 10H_2O$) [22], and it is this one that causes a relatively high supersaturation level and crystallization pressure during the evaporation and recrystallisation of Na_2SO_4 [23-28]. Ruiz-Agudo et al. [29] have put forward a theory of deterioration by salts in adsorption. Magnesium sulfate ($MgSO_4$) has a high adsorption capacity and damages the rock surface by causing layer separation; sodium sulfate (Na_2SO_4), being less adsorptive, diffuses deeper into the rock and forms a wide-scale structure crack. The Extent of salt-induced damage is also relatively sensitive to the evaporation environment. Damage caused by a low relative humidity and rapid evaporation is generally more severe than that caused by a high relative humidity and slow evaporation [30]. Many of the stone cultural relics in China have been damaged by saline-alkali degradation. For example, about 20% of the caves in Mogao Grottoes of Dunhuang have been damaged by salt weathering to different extents. Salt-crystallization damage is widespread at Beishan Grottoes in Dazu, Sichuan. Analysis shows that the two main salts causing efflorescence-related damage in Cave 276 of Mogao Grottoes are SO_4^{2-} and Cl^-. Liu and others [31] showed that surface salt-alkali weathering in Yungang Grottoes is responsible for about 31.67% of the total pollutant-damaged area. Given the above problems, to preserve the stone cultural relics for a longer time, it is necessary to prevent saline-alkaline damage and take salt-removal measures.

Field investigation of the Han white jade (HWB) railings at BeiYue Temple in Quyang shows widespread salt weathering and severe areas of salt-alkali damage. The surface of the marble showed all sorts of damage caused by soluble salts and was therefore in a desperate state of deterioration. Traditionally, most desalination methods have been based on physical adsorption; that is to say, salt ions are extracted from the surface and pores of the stone material and subsequently transferred to the desalting medium. Intermolecular Van der Waals forces are responsible for this process; therefore, salt ions are weakly attracted to and temporarily bound within the fibre structure of rice paper or other absorbent materials. However, this way has several deficiencies, such as a low desalination rate, high material and labour costs, poor salt-removal efficiency, and insufficient preservation effects. Therefore, the long-term damage from soluble salt corrosion to the cultural relics will also continue. Many desalting materials are available in a commercial scale, and most of the older methods use deionized water as the medium. It is a water-molecule-permeability and diffusion-based mode of action that separates salt from the fibers. However, new composite modifier-based desalination materials have recently begun to be introduced. The modifier helps regulate the rate of crystal growth by changing supersaturation, improves the solubility of salts, and is coordinated with the carboxyl group (-COOH). They can work in conjunction with surfactants to modify the crystal structure of salts and accelerate desalinisation. At present, the three main aims of research on desalination materials for heritage protection are enhanced adsorption performance, cost-effectiveness and conservation efficiency. Chen [34] has shown that composite modifiers with a ratio of 1:2 and 1:3 are better than other types in enhancing desalination rates. Building on the above results, the three different modifier ratios of 1:2, 1:2.5 and 1:3 were also selected for experimental studies on desalination efficiency. Investigate how changes in different concentrations affect the extraction rate of salt and thus find a modified construction method to make use of marble

waste in seawater desalination.

2 Methods

2.1 Experimental Materials and Principles

To enhance the desalinisation efficiency of stone cultural relics, improve the salt-extraction rate of traditional materials, and reduce further damage due to soluble-salt weathering, this paper will put forward a desalinisation strategy that meets the conservation requirements for heritage protection. Polyacrylic acid (PAA) [32, 33] (as a growth regulator) and polyepoxysuccinic acid (PESA) [34] were selected as compound modifiers for the treatment of Na_2SO_4 contamination, and crystallization modifiers [35, 36] were added to regulate the dynamics of salt nucleation by functioning as nucleation inhibitors (preventing crystal formation), nucleation promoters (facilitating controlled crystallization within the rock matrix), and habit modifiers (altering crystal morphology to enhance salt removal). Add the above modifying terms to the existing adhesive-desalination treatment for testing. Salt-crystallization modifiers regulate the nucleation and growth rate of inorganic salts, change crystal shape, increase supersaturation in soluble salt solutions, extend the induction period for crystallization, and promote migration and extraction of salts from the inside to the outside of stone relics.

In the absence of an acid, -COOH in PAA and PESA lose a proton (H^+) and form carboxylate ions (COO^-); this is called deprotonation. Water molecules will be present to help dissociate the proton, shift the dynamic equilibrium towards deprotonation, and thus increase the proportion of -COOH that has lost H^+.

Similarly, $-COO^-$ in PAA and PESA also deprotonate under neutral conditions; water molecules interact with these groups to further promote H^+ dissociation and generate more COO^-. This is a spontaneous equilibrium, and at a neutral pH, deprotonation will occur to some extent; thus, the concentration of COO^- will be relatively high. Aqueous solution dissociates fully into Na^+ and SO_4^{2-} ions. After PAA and PESA are deprotonated, the oxygen atoms in the resulting $-COO^-$ group have lone pairs of electrons, and Na^+ ions are electron-deficient. Electron configuration can form coordination bonds to produce the special interaction among PAA, PESA and Na_2SO_4. PAA and PESA inhibit the growth of crystal faces, and thus change the shape of Na_2SO_4 crystals. The above compounds are synergistic and regulate the growth rate of crystals along different axes to induce changes in crystal morphology during crystallization. Therefore, Na_2SO_4 crystal structures have been modified to reduce the risk of structural damage to stone relics. Chen and Zhao [37] put forward that with a PAA-PESA ratio of 1:2 or 1:3, the efficiency of desalination and the structure of salt crystals can be improved; however, the optimal actual experimental results have not yet been obtained. Therefore, three PAA-PESA ratios (1:2, 1:2.5 and 1:3) were selected for investigation in this paper. The above formulas were added to the traditional desalination materials of rice paper and desalination pulp, and then their salt-removal efficiency in controlled desalination experiments was tested.

2.1.1 Material Properties

The main materials in this study are PAA, PESA and sodium hydroxide (NaOH).

(1) PAA: The PAA solution in this paper was supplied by Shanghai Maikelin Biochemical Technology Co., Ltd. A light-yellow liquid that is easily dissolved in both water and organic solvents, and is non-toxic. The density at 20 °C is 1.09 g/cm³. Poly(acrylic acid) (PAA) is often used as a scale inhibitor and dispersant to chelate hardness ions, such as Ca^{2+} and Mg^{2+}, and thus inhibit scale formation. It can also spread suspended particles in an aqueous system to keep the water system clear. PAA forms a stable complex with metal ions such as Ca^{2+} and Mg^{2+}, and

has good decomposition properties for calcium carbonate ($CaCO_3$) and calcium hydroxide ($Ca(OH)_2$) in aqueous solution. The solution is a weak acid with a pKa of 4.75, and it will decompose thermally at temperatures over 300 °C. Structurally, PAA contains -COOH and carbon-carbon double bonds (C=C); thus, it can be modified in solution by intermolecular interactions and the breaking and reforming of its chemical bonds. The modified solution is relatively more saturated, so the desalination reaction proceeds more quickly and has a higher overall desalination rate.

(2) PESA: The PESA solution in this study was also supplied by Shanghai Maikelin Biochemical Technology Co., Ltd. A light-brownish liquid with good solubility in both water and organic solvents that is non-toxic is referred to as an aqueous-alcohol system. It is 1.28 g/cm^3 in density and between 9 and 12 on a pH scale at 20 °C. PESA is an effective scale and corrosion inhibitor that suppresses the growth of $CaCO_3$ and calcium sulfate ($CaSO_4$) scales in water. Prevent corrosion of metal equipment and extend its service life simultaneously. The first purpose of making a PESA solution is to reduce its viscosity and speed up the rate of desalinisation reactions, in line with PAA.

(3) NaOH: Add NaOH to change the pH during desalination. Release of hydroxide ions (OH^-) serves to increase the pH.

2.1.2 Reagent Preparation

The ratios of reagent preparation are shown in Table 1. PAA and PESA were mixed at ratios of 1:2, 1:2.5 and 1:3 to prepare the modified solutions, and a final concentration of 0.3% for the active agents was achieved. Add an NaOH solution to raise the pH of the medium back to 7 and maintain this pH.

Table 1: Proportions and pH of Reagent Solutions

Material	Proportion	pH
PAA-PESA	1:2	7
PAA-PESA	1:2.5	7
PAA-PESA	1:3	7

Table 2: Experimental Ratios of Applied Desalination Materials

Material	pH	Christen
Paper+125ml0.3%1:2PAA-PESA	7.31	A
Paper+125ml0.3%1:2.5PAA-PESA	7.28	B
Paper+125ml0.3%1:3PAA-PESA	7.32	C
Paper+125ml Deionized water	7.19	D
Pulp+125ml0.3%1:2PAA-PESA	7.58	E
Pulp +125ml0.3%1:2.5PAA-PESA	7.76	F
Pulp +125ml0.3%1:3PAA-PESA	7.64	G
Pulp +125ml Deionized water	7.70	H

Rice paper was cut into 80 mm × 80 mm squares and immersed in 125 mL of the following solutions, as shown in Table 2: 0.3% 1:2 PAA-PESA, 0.3% 1:2.5 PAA-PESA, 0.3% 1:3 PAA-PESA, and deionized water. The four labelled samples are A, B, C and D.

Four samples of desalting pulp, each 125g in weight, were weighed on a balance. For each part, 125 mL of 0.3% 1:2 PAA-PESA, 0.3% 1:2.5 PAA-PESA, 0.3% 1:3 PAA-PESA and deionized water were added, and the corresponding samples were labelled as E, F, G and H.

NaOH was added to raise the pH of the solutions to a neutral level, and at this time, the pH

values of all the prepared solutions were measured and recorded.

2.1.3 FTIR Analysis

Figure 1 is a Fourier-transform infrared (FTIR) spectrum, and several characteristic absorption peaks of various functional groups are shown. At a 1:2 PAA-PESA ratio, the absorption peak at 3369.49 cm^{-1} is due to O-H stretching vibration, and the peak at 2945.07 cm^{-1} is that of methylene (CH_2) stretching vibration. The maximum around 1591.34 cm^{-1} is assigned to the C=O stretching vibration, and the band at 1391.50 cm^{-1} is a methyl (CH_3) stretching vibration. A C-O-C bond stretching vibration at 1216.47 cm^{-1} has also appeared. The characteristic absorption peak of PAA is at 1106.55 cm^{-1}, and the O-H deformation absorption peak in -COOH appears at 1067.38 cm^{-1}. As the PAA-PESA ratio increases from 1:2 to 1:2.5, the absorption peaks for PESA at 2951 cm^{-1} (CH_2 stretching vibration) and 1216 cm^{-1} (C-O-C stretching vibration) gradually decrease, while the peaks corresponding to PAA at 1389.8 cm^{-1} (CH_3 stretching vibration), 1109.30 cm^{-1}, and 1066.63 cm^{-1} (O-H deformation in -COOH) become relatively stronger. When the PAA ratio is further increased from 1:2.5 to 1:3, the FTIR spectra of both components converge and show almost the same absorption pattern.

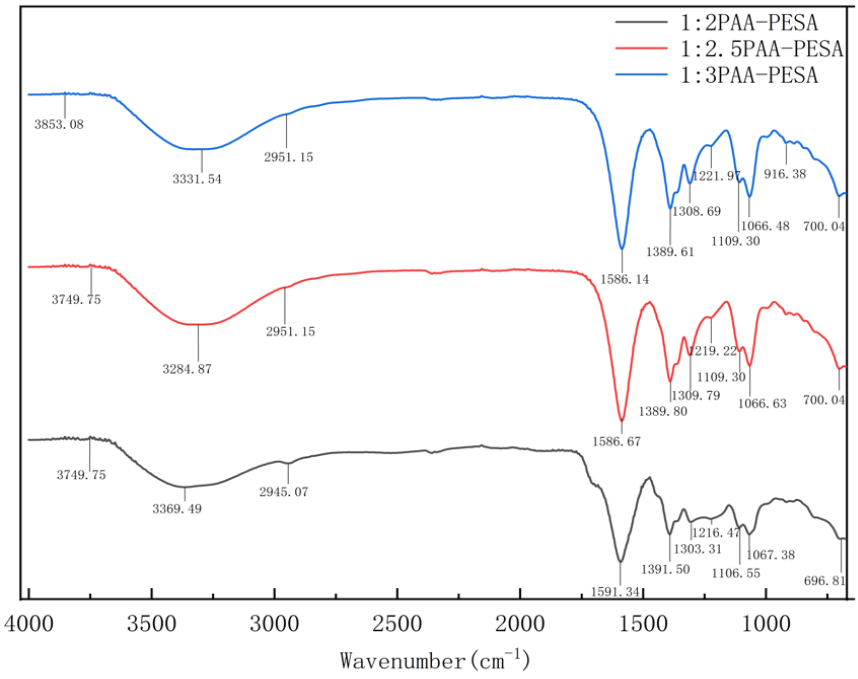

Figure 1: FTIR spectra of PAA and PESA at different ratios

2.2 Experimental Procedures

The areas that were severely damaged by salt on the stone railings were the first to be identified and designated as desalinisation zones. Eight regions of 80 mm $\times$ 80 mm each were marked with yellow adhesive tape to ensure the accuracy of the treatment area. Only a soft-bristle brush is used for light cleaning of the top layer to avoid damaging the desalinisation surface. The first four sections are rice paper, and the last four sections are desalination pulp. For each application of rice paper or desalination pulp, allow it to be in contact with the soluble salts for 8 hours. To achieve full desalinisation, all eight treated areas were subjected to multiple desalination cycles, and the number of times this operation was repeated for impact assessment over time reached 14.

2.3 Testing Methods

2.3.1 Morphological Observation

Macro and micro images of the stone surface before and after desalinisation were taken with a single-lens reflex (SLR) camera and an Anyty 3R portable digital microscope. An SLR camera is used to photograph changes in colour of the surface of the stone and to check for any remaining pulp or rice-paper deposits after desalination. A portable digital microscope that could magnify the objects up to 200× is used for observations of the inside of the crystal in this stone and to determine whether any significant alterations to its structure have occurred after desalination.

2.3.2 Conductivity Test

A DDS-307A conductivity meter (DS-307A) was selected to conduct the measurement of conductivity in the desalination experiment. Measure the ease of charge transport in the solution and, thereby, determine the total concentration of extracted anions and cations from the stone as well as the total concentration of salts. Conductivity measurements can directly reflect the efficiency and desalination rate achieved by the three materials in desalination. Monitor the changes in conductivity to observe whether desalination is occurring; when these changes no longer occur, then it can be assumed that desalination has finished.

The steps of the experiment are as follows: The obtained dried pulp and rice paper samples after desalination were first placed in a beaker, and then 60 mL of deionized water was added. Let the sample stand for one hour after adding it, and then completely dissolve any that have not dissolved before measuring conductivity. A total of 14 cycles have been carried out for desalination treatment.

2.3.3 Ion Chromatography

Determine the types and strengths of ions in the desalination solution using ion chromatography, and the results are presented in Table 3. In accordance with the provisions of the "Austrian Technical Standard B3355-1: Trockenlegung von feuchtem Mauerwerk - Teil: Bauwerksdiagnostik und Planungsgrundlagen", rice paper and pulp samples of the four tested materials were ionised at key stages of the desalinisation process: the first desalinisation cycle, after the end of desalinisation, the last desalinisation cycle, and at the point with the highest conductivity values during desalinisation.

Table 3: Standardized Salt Concentration Ranges for Stone Weathering Classification

Types of ions /wt.%	Cl^-	NO_3^-	SO_4^{2-}
Mild salt weathering	≤0.03	≤0.05	≤0.10
Moderate salt weathering	0.03~0.10	0.05~0.15	0.10~0.25
Severe salt weathering	≥0.10	≥0.15	≥0.25

A Thermo Scientific Aquion Ion Chromatograph was used for the ion chromatography test, and an AS-DV automatic sampler, a conductivity detector, a Dionex AERS 500 4mm anion suppressor, a Dionex IonPac™ AS22 (4×250 mm) anion column, a Dionex CSRS 300 4mm cation suppressor, and a Dionex IonPac™ CS12A (4×250 mm) cation column were employed. The other instruments in the laboratory for this study include an Ohaus electronic balance (CP423C) for weighing samples, a BECKMAN COULTER Allegra 64R centrifuge, and a Chengdu Haocun Instrument Ultra-Pure Water System (KMCC-AIII-10B).

The test steps are as follows: First, accurately weigh the sample and record all the data

precisely. The desalinated pulp and rice paper samples were then placed in 10 mL of ultra-pure water and allowed to soak for a set time to dissolve the soluble salts. Soak the sample in water, and then, for 20 minutes at 40 °C, use an ultrasonic bath to disperse it. Second, at 6000 rpm for 15 minutes, the treated samples were centrifuged to separate suspended solids from the liquid phase. Filter the top clear liquid of the supernatant to remove suspended solids, and then carry out ion chromatography analysis.

2.3.4 XRF

Samples were collected from both the desalinated and non-desalinated areas of the four materials applied with pulp, and a comparative analysis was conducted based on the results of the previously mentioned tests. X-ray fluorescence (XRF) analysis was also conducted on the parts where the pulp adhered well and the extent of desiccation was determined. A Rigaku ZSX Primus IV XRF diffractometer was used to perform XRF analysis of the stone, and at this time, its main chemical components were determined. A comparison of the elemental composition of the stone before and after desalination was carried out. In addition to identifying the main mineral components, XRF analysis was also carried out to study the internal composition of the stone, and especially the concentration of SO_4^{2-} and sulfides was determined.

2.3.5 XRD

Samples were taken from both the desalinated and non-desalinated regions of the four materials treated with pulp, and these were compared with the results of prior experiments. XRD analysis was also performed on the structural changes induced by desalination in the area of the pulp material with good adhesion. XRD analysis seeks to know whether there is a change in the crystal structure of Quyang Hanbaiyu marble after desalinisation, and also to determine if there have been any structural damage or other modifications caused by the treatment. XRD tests were conducted with a Rigaku SmartLab SE diffractometer, a copper target (Cu Kα radiation) was used, and the following operating conditions were employed: scan range of 5° to 90° and a scan speed of 10°/min.

3 Results

3.1 Morphological Observation

As shown in Figure 2, after desalinisation treatment of the macroscopic shape of the rice paper-treated stone surface, there is a significant decrease in yellow impurities due to the four test materials. Based on the above, it is inferred that self-cleaning occurs, and after desalinisation treatment, the surface of the stone is visibly cleaner, with no remaining rice paper present. Based on the microscopic shape analysis before and after desalinization, the internal structure of the stone is denser; thus, it can be concluded that the desalination solution does not cause damage to the microstructure of the stone. Among the materials that have been tested, Material A was able to reduce both black particulate pollutants and yellow surface residues most significantly after desalting. Materials B and C had a relatively small number of black particulate contaminants, and yellow residues were still visible on the surface. Material D had a relatively large amount of residual black particulate contamination. According to the four materials, A, B and C performed better in terms of desalination and cleaning than D. Material A performed the best overall among them and significantly reduced both black and yellow contaminants.

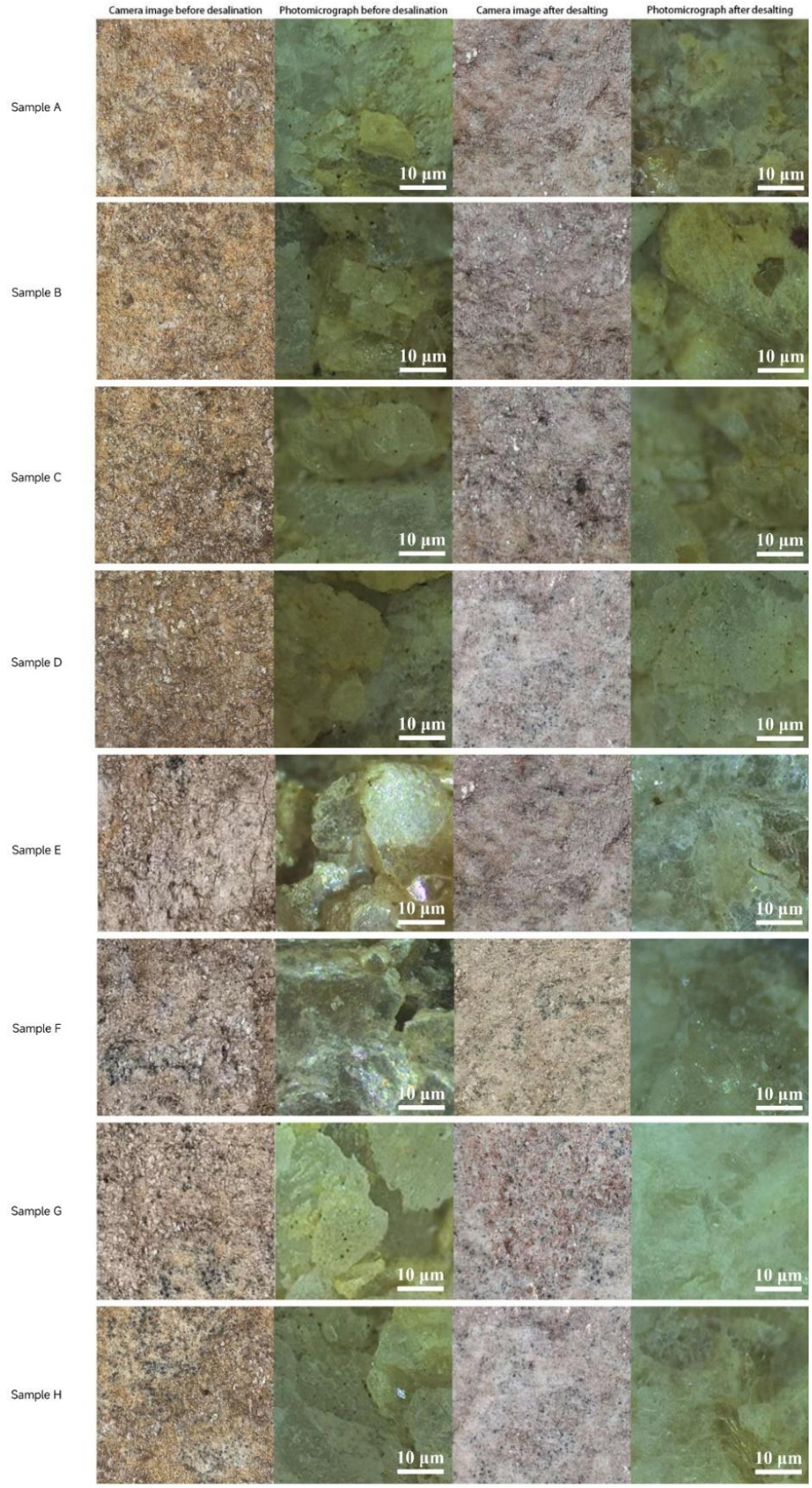

Figure 2: Macroscopic and microscopic morphological changes before and after desalination

Based on a comparison of the macroscopic images before and after desalination with paper pulp, it was found that the surfaces of Materials E, F, G, and H were free of yellow contaminants after treatment. The stone surfaces were lighter in colour and exhibited a relatively strong self-cleaning property. No leftover paper pulp was left on the stone surface after desalination either. Microscopic images show that the internal structure of the stone is undamaged after desalination, and therefore no damage to the micro-structure has occurred due to the desalination solution. Material E has a clean surface now and no black or yellow spots of contamination. However, black particulate contaminants were still present in Materials F and G within the stone after desalination. Material H retained yellow contaminants on its surface and was therefore not salt-free. Based on the above tests, Materials E, F, and G were superior to Material H in both desalination and cleaning performance, and the stone's internal structure was also relatively clean after desalination.

In short, the added modifiers effectively reduced the amounts of both black and yellow stains during desalinisation, thus making the stone surfaces lighter and cleaner.

Comparing the desalination performance of rice paper and paper pulp, it was found that the modifier-containing materials had significantly enhanced desalting and cleaning capabilities compared with the control group. Material A and Material E had good desalination and cleaning performance, but Material E was the best overall.

Finally, the desalination pulp was selected as the basic material and, in combination with a 1:2 PAA-PESA solution, achieved good desalination results without the introduction of new impurities during treatment.

3.2 Conductivity Test

Figure 3(a) and 3(b) are the conductivity test results of rice paper and desalting pulp after 14 cycles of desalination.

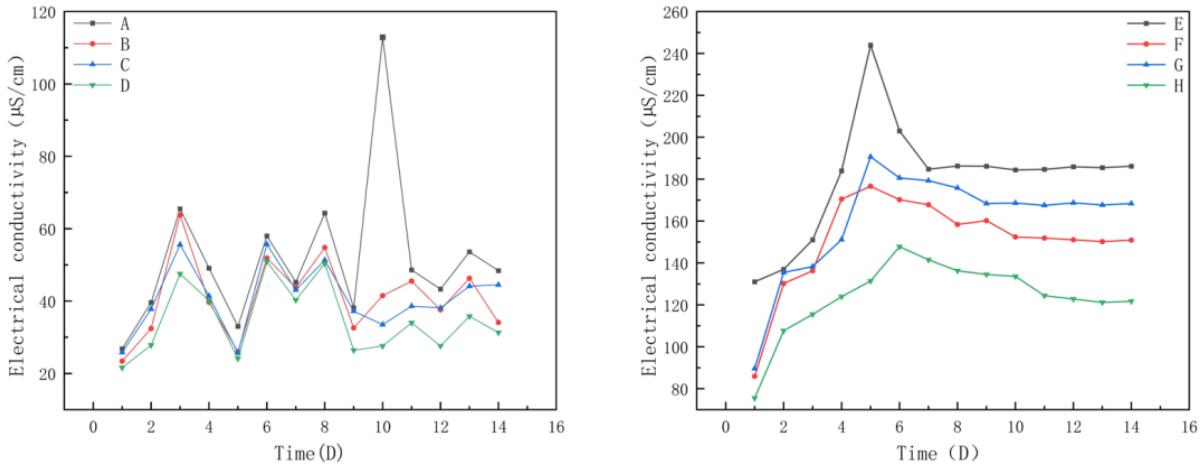

(a):Conductivity value for desalting of rice paper (b):Pulp desalination conductivity value

Figure 3: Conductivity measurements of rice paper and pulp during desalination

As shown in Figure 3(a), none of the four test samples have been desalinated yet, and their conductivity values are still fluctuating during the test. Among the materials that were tested, Material A had the best desalting performance; that is to say, after 10 cycles, it had a conductivity of 112.9 μS/cm and thus removed the largest amount of salt. Materials B and C had relatively higher conductivity values and improved salt-rejection performance compared with Material D.

Figure 3(b) shows the conductivity test results of the desalting pulp, and it can be seen from

this that all four groups have been fully desalted; the conductivity values have also stabilized by the 14th cycle. Among them, the three pulp samples that added crystalline modifiers showed good desalting results compared with the control sample without modifiers. Among the modified materials, Material A showed the best desalination performance and reached a conductivity of 244 μS/cm after five cycles; therefore, it was determined that it had the highest desalination rate. Conductivity stabilized after the 6th cycle, and desalination of this sample was thus achieved. Material G had a lower conductivity than Material F on the 4th day, but by the 5th day, its maximum conductivity of 190.7 μS/cm had been reached. Then the conductivity value dropped gradually, and by the 9th day, desalinisation was finished. The maximum conductivity of Material F was 176.6 μS/cm on the fifth day, but it had shown considerable fluctuations and was thus less stable in terms of desalination. Conductivity gradually stabilized after the 10th day and was thus one of the lower desalinisation rates for the modified samples. Sample H, the control group without modifiers, showed the lowest peak conductivity of 147.8 μS/cm on the 6th day, and by the 12th day it had stabilized, indicating the end of desalination.

In short, by comparing the conductivity values after desalination using rice paper and desalting pulp, Material A among the rice paper samples had the highest conductivity; it was determined that this showed successful salt removal, and Materials B and C, although having lower conductivity values, also removed more salt than Material D, thus indicating that B and C were more effective at desalination. Among the desalting pulp materials, Material E showed the highest desalination rate; by the 7th day, it had achieved desalting with a conductivity value of 244 μS/cm and thus exhibited the most effective salt removal. Material F was desalinated on the 10th day and reached a maximum conductivity of 176.6 μS/cm; Material G had been desalinated by the 9th day and showed a higher maximum conductivity of 190.7 μS/cm. Material H (control sample) had the lowest desalination rate, was fully desalted by the 12th day, and reached a maximum conductivity of 147.8 μS/cm. The materials that added composite modifiers had a significantly higher conductivity than those that were treated with deionized water; therefore, they could improve salt extraction, and when applied to pulp, they performed better in desalting than those used for rice paper, suggesting they are a more effective carrier for desalination treatments. Among all the tested materials, Material E had the highest conductivity after desalination, the highest desalination rate, and thus the best overall desalination performance. In addition, among the above, the 1:2 PAA-PESA solution was the best for preparing the desalting pulp-based base material.

3.3 Ion Chromatography Test

Figure 4(a)-4(c) show the changes in the concentration of NO_3^-, SO_4^{2-} and Cl^- in rice paper before and after desalination, and Figure 4(d)-4(f) show the corresponding changes in ion concentration in desalting pulp after treatment with eight different materials.

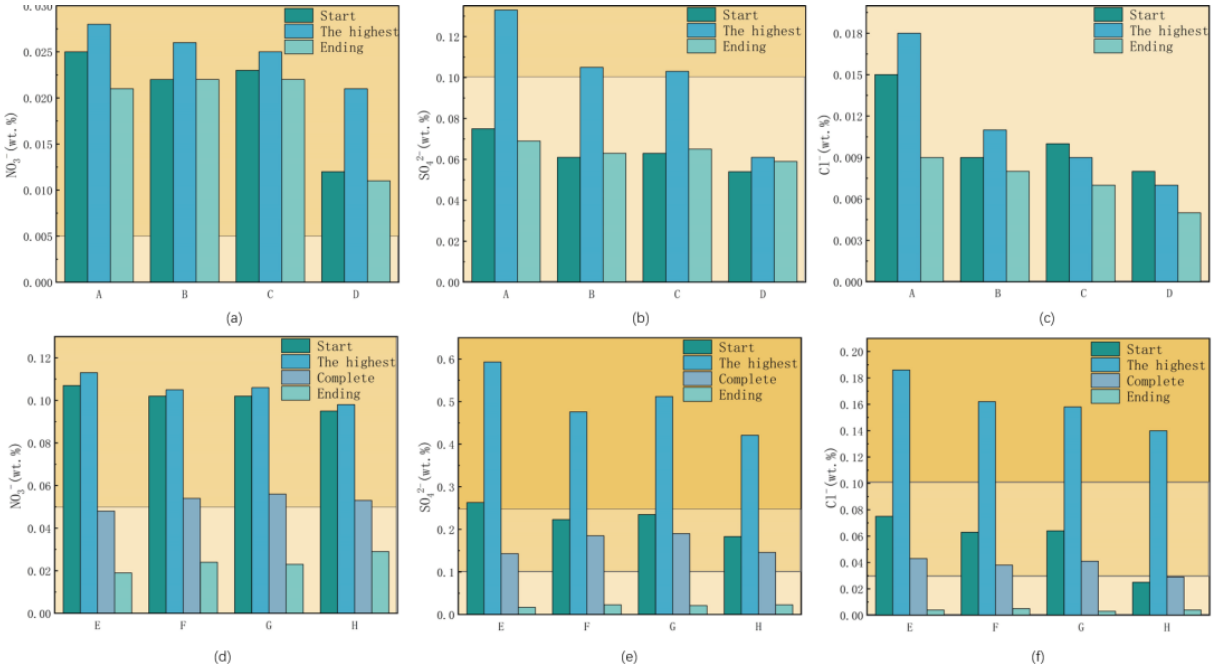

Figure 4: Anion concentration changes in desalination treatments

Figure 4(a) shows the change in NO_3^- concentration in rice paper after desalination. Based on the above data, the three material groups containing composite modifiers showed better desalting efficiency than the control group. At the start of the desalination process, Material A had an initial NO_3^- concentration of 0.025 wt.%. At this time, the concentration had reached a peak of 0.028 wt.% and had subsequently fallen to 0.02 wt.% after the last desalination step. According to the final NO_3^- concentration, the internal salt weathering degree of the stone was classified as moderate.

Figure 4(b) shows the change in SO_4^{2-} concentration of rice paper after desalination. Based on the above data, all three materials containing composite modifiers demonstrated a superior rate of SO_4^{2-} removal compared to the control group. At the start of the desalination process, Material A had an initial concentration of 0.075 wt.% for SO_4^{2-}. At the maximum during the desalination process, the concentration was 0.133 wt.%, and it gradually dropped to 0.069 wt.% after the last desalting cycle. Based on the final concentration of SO_4^{2-}, the internal concentration of SO_4^{2-} in the stone was classified as light salt weathering, and little SO_4^{2-} accumulation occurred after desalination.

Figure 4(c) shows the changes in Cl^- concentration in the rice paper during desalination. Based on the above experiments, materials containing composite modifiers have achieved better desalting performance than the control group. At the beginning of desalination, Material A had an initial Cl^- concentration of 0.015 wt.%. At the same time, the concentration reached a maximum of 0.018 wt.% in this step, and by the end of the last desalination cycle, it had increased to 0.09 wt.%. Although it rose to some extent, the Cl^- content of the stone was still in the light-salt-weathering range.

Figure 4(d) shows the change in NO_3^- concentration during desalination by pulp. The results are the same as for rice paper; materials with composite modifiers also showed better desalting performance than the control group. At the start of the desalination process, Material E had an initial NO_3^- concentration of 0.107 wt.%. At the end of desalination, the concentration was about 0.048wt% and had reached a maximum of 0.113wt%. In the last desalination cycle, the concentration of NO_3^- was further reduced to 0.019 wt.%, and the internal NO_3^- content of the stone was thus classified as light salt weathering.

Figure 4(e) is the change in SO_4^{2-} concentration of pulp during desalination. Based on the above experiments, all three materials with composite modifiers performed better in the removal of SO_4^{2-} compared to the control group. At the beginning of desalination, Material E had an initial concentration of SO_4^{2-} as 0.263 wt.%. At this time, the maximum concentration reached was 0.593 wt.%, and it subsequently dropped to 0.143 wt.% by the end of the desalting cycle. In the last desalting cycle, the concentration of SO_4^{2-} was further reduced to 0.017 wt.%, and the internal SO_4^{2-} content of the stone was classified as light salt weathering; thus, the accumulated SO_4^{2-} after desalination was minimal.

Figure 4(f) shows the changes in Cl^- concentration of pulp during desalination. Materials with composite modifiers also showed good desalting performance compared to those in the control group, in line with other trends for ions. Material E had an initial concentration of Cl^- at 0.075 wt.% at the start of desalination. The maximum concentration reached was 0.186 wt.%, and it then gradually dropped to 0.043 wt.% at the end of desalting. In the final desalting cycle, the concentration of Cl^- was reduced further to 0.004 wt.%, and the amount of Cl^- was significantly decreased. At first, the stone was classified as heavily salt-weathered. Desalination reduced the concentration of Cl^- to a level that falls under the classification of light salt weathering, and therefore little Cl^- accumulation occurred.

The composite modifier in this study has some functional groups, such as amine groups (-NH_2) and -COOH, and helps to improve the desalination performance. These functional groups form stable chelates with metal ions in the pulp and thus lead to the formation of larger molecular structures or compounds with altered solubility. The above method effectively reduces the rate of crystal face growth and causes a directional difference in the growth rate of Na_2SO_4 crystals. Therefore, the shape of the Na_2SO_4 crystals has changed, and as a result, the interface between the pulp and salt ions is reduced. As a result, the salt ions detach more readily from the stone surface and are effectively absorbed by the pulp to speed up the desalination process and improve salt removal efficiency.

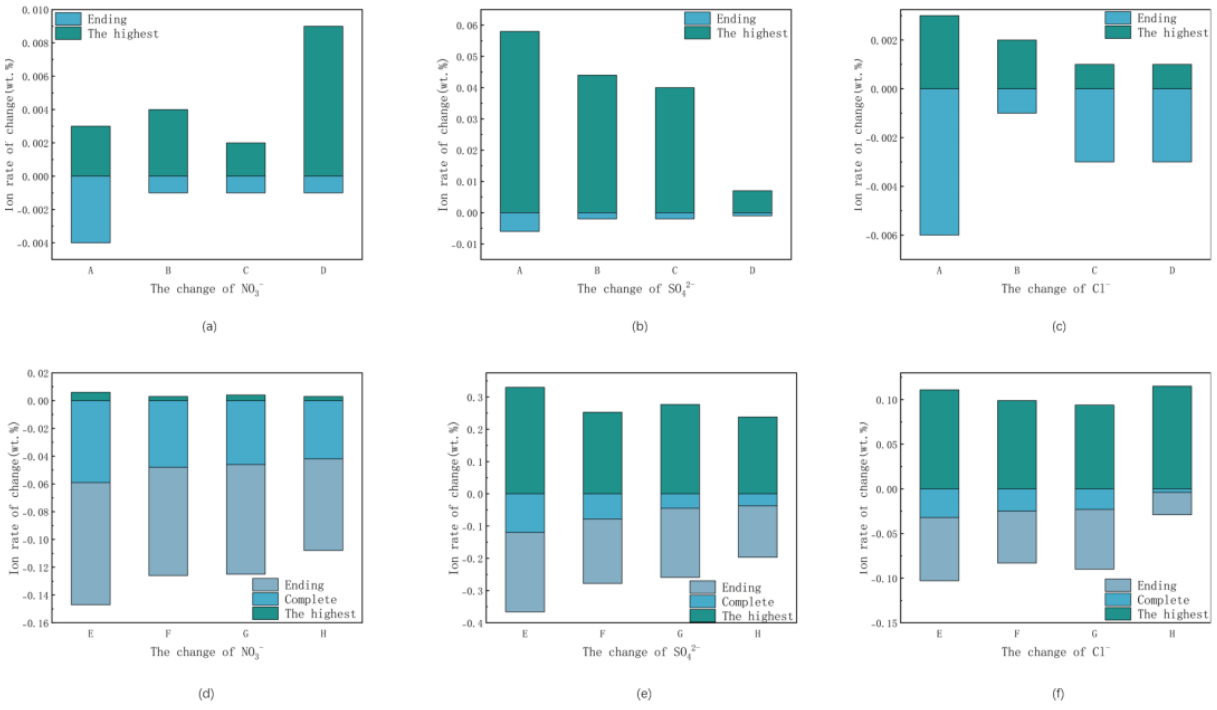

Figure 5: Rate of anion concentration change after desalination treatment

Figure 5(a)-5(c) shows the rate of change in ion concentration of rice paper after

desalination.

Figure 5(a) shows the change in NO_3^- concentration after desalination. Among the tested materials, Material A (1:2 PAA-PESA) had the highest initial concentration at 0.028 wt.%, and after the first desalting cycle, it dropped to 0.02 wt.% in the end. The control group (Material D) reduced by 0.021 wt.% to 0.011 wt.%, so its desalting efficiency was relatively low. Materials B and C both had intermediate performance, and their final NO_3^- concentrations were 0.021 wt.% and 0.022 wt.%.

Figure 5(b) shows the change in SO_4^{2-} concentration after desalination. Material A had a relatively high concentration of SO_4^{2-}, up to 0.133 wt.%, and then fell to 0.069 wt.% after being subjected to desalination. The control group (Material D) showed a relatively small reduction, decreasing only slightly from 0.061 wt.% to 0.053 wt.%, and thus had a lower removal rate of SO_4^{2-}. Desalination reduced the SO_4^{2-} content in the stone, and thus it was downgraded from "moderate salt weathering" to "light salt weathering".

Figure 5(c) is the change in Cl^- concentration after desalination. Material A had the highest concentration of Cl^- at that time, up to 0.018 wt.%, and then fell to 0.09 wt.% later on. The control group (Material D) only had a small decrease, from 0.009 wt.% to 0.005 wt.%.

Figures 7(e) - 7(g) show the rate of change in ion concentration of pulp after desalination.

Figure 7(e) shows the change in NO_3^- concentration after desalination. Material E (1:2 PAA-PESA) had the highest initial NO_3^- concentration of 0.113 wt.% and then dropped to 0.019 wt.% at the end of the desalination process. The control group (Material H) showed a weaker effect of NO_3^- removal; its concentration decreased from 0.098 wt.% to 0.029 wt.%, and thus had a lower desalting efficiency. Materials F and G had medium-level performance, and their final NO_3^- concentrations were 0.024 wt.% and 0.023 wt.%, respectively.

Figure 7(f) shows the change in SO_4^{2-} concentration after desalination. Material E (1:2 PAA-PESA) had the highest initial SO_4^{2-} concentration, reaching a maximum of 0.593 wt.%, and then dropped to 0.017 wt.% at the end of the desalination process. On the other hand, the control group (Material H) showed a smaller decrease; the concentration of SO_4^{2-} dropped from 0.421 wt.% to 0.023 wt.%, and its removal rate for SO_4^{2-} was thus lower. After desalinisation, the SO_4^{2-} content of the stone was reclassified from "severe salt weathering" to "light salt weathering".

Figure 7(g) shows the change in Cl^- concentration at different times during desalination. Material E had a high Cl^- content, reaching a maximum of 0.186 wt.% and then falling sharply to 0.004 wt.% after the last desalting cycle. The control group (Material H) also showed Cl^- removal, and the concentration decreased from 0.14 wt.% to 0.004 wt.%.

Add a composite modifier and then improve the removal rates of all target ions. Among the test formulations, the 1:2 PAA-PESA ratio performed better in both rice paper and pulp-based treatments for desalination. On the other hand, the control group showed a small change in ion concentration; thus, the modifier did not increase the supersaturation of the salt solution and therefore was less effective in promoting salt extraction. Desalination was carried out to reduce the salt content of the stone to the level of "light salt weathering"; thus, the accumulation of soluble salts was significantly reduced and met the requirements for cultural heritage conservation.

In short, the above experimental data show that the desalting pulp outperformed conventional rice paper in desalination capacity, and the addition of modifier solutions further boosted the salt-removal rate compared to the control sample. Ion chromatography analysis showed that the 1:2 PAA-PESA composite modifier could effectively remove soluble salts (NO_3^-, SO_4^{2-}, Cl^-) from HWB body, and achieved a high desalination rate and a large total salt removal compared with other tested ratios and traditional methods.

3.4 XRF

As shown in Figure 6, the principal minerals on the stone surface are mainly calcium oxide (CaO), with a relatively small proportion of sulfur trioxide (SO_3) and silicon dioxide (SiO_2). Before desalination, CaO and SiO_2 in the stone were around 95 wt.% and 0.35 wt.%, respectively, and other components, such as SO_3, were approximately 0.9 wt.% and 0.3 wt.%. Desalination was performed, and then the concentrations of CaO and SiO_2 reached 96 wt.% and 0.4 wt.%. In all the tested samples, an increase in the amount of CaO has been observed, indicating that during desalination, other soluble components have been removed and thus CaO has been relatively enriched in the stone matrix. In addition, all the samples showed a significant decrease in SO_3 after desulfurization, and thus the sulfide-containing compounds on the stone surface had been removed by this treatment.

Sample A	Oxide content (wt.%)							
Schedule	CaO	SO_3	SiO_2	MgO	Fe_2O_3	K_2O	Al_2O_3	P_2O_5
Before desalination	95.132	0.321	0.392	1.152	1.004	0.072	0.133	0.211
After desalination	96.548	0.143	0.454	0.987	0.964	0.053	0.152	0.197

Sample B	Oxide content (wt.%)							
Schedule	CaO	SO_3	SiO_2	MgO	Fe_2O_3	K_2O	Al_2O_3	P_2O_5
Before desalination	95.815	0.305	0.405	1.137	1.021	0.064	0.131	0.194
After desalination	96.588	0.152	0.434	0.876	0.978	0.058	0.134	0.187

Sample C	Oxide content (wt.%)							
Schedule	CaO	SO_3	SiO_2	MgO	Fe_2O_3	K_2O	Al_2O_3	P_2O_5
Before desalination	95.457	0.324	0.387	1.145	0.998	0.068	0.135	0.201
After desalination	96.264	0.167	0.411	0.897	0.988	0.062	0.128	0.187

Sample D	Oxide content (wt.%)							
Schedule	CaO	SO_3	SiO_2	MgO	Fe_2O_3	K_2O	Al_2O_3	P_2O_5
Before desalination	95.359	0.318	0.395	1.197	1.017	0.064	0.133	0.199
After desalination	95.889	0.292	0.418	0.887	0.996	0.061	0.125	0.189

Sample E	Oxide content (wt.%)							
Schedule	CaO	SO_3	SiO_2	MgO	Fe_2O_3	K_2O	Al_2O_3	P_2O_5
Before desalination	95.265	0.315	0.389	1.168	0.989	0.061	0.138	0.187
After desalination	97.784	0.005	0.468	0.785	0.647	0.032	0.078	0.124

Sample F	Oxide content (wt.%)							
Schedule	CaO	SO_3	SiO_2	MgO	Fe_2O_3	K_2O	Al_2O_3	P_2O_5
Before desalination	95.458	0.315	0.379	1.147	0.884	0.056	0.129	0.185
After desalination	96.332	0.014	0.466	0.895	0.546	0.038	0.078	0.129

Sample G	Oxide content (wt.%)							
Schedule	CaO	SO_3	SiO_2	MgO	Fe_2O_3	K_2O	Al_2O_3	P_2O_5
Before desalination	95.367	0.310	0.396	1.158	0.896	0.052	0.137	0.189
After desalination	96.565	0.018	0.472	0.801	0.598	0.036	0.081	0.125

Sample H	Oxide content (wt.%)							
Schedule	CaO	SO_3	SiO_2	MgO	Fe_2O_3	K_2O	Al_2O_3	P_2O_5
Before desalination	95.712	0.309	0.359	1.157	0.749	0.061	0.124	0.179
After desalination	97.457	0.058	0.472	0.842	0.531	0.042	0.076	0.124

(a)

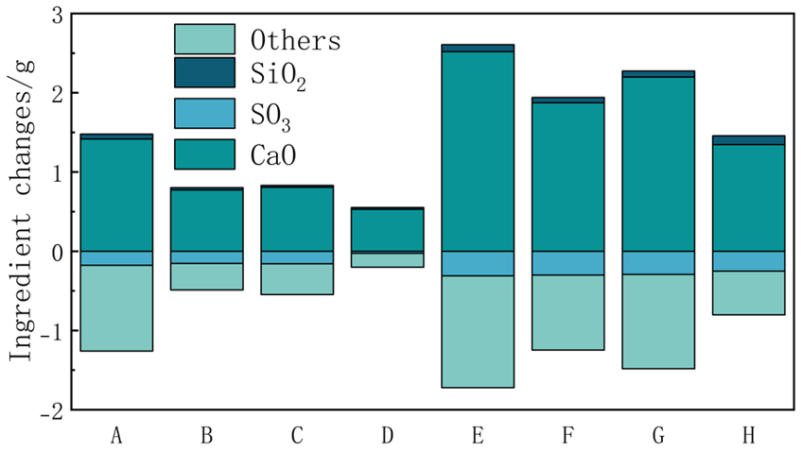

(b)

Figure 6: XRF analysis of major elemental components before and after desalination

XRF composition changes before and after desalination for the eight test samples show that they have been cleaned to a certain extent. Comparing materials A, B, C and D shows that material A reduced the level of surface contamination the most; thus, it has a clean and stable stone surface. Notably, SO_3 content dropped significantly, and the concentrations of CaO and SiO_2 rose moderately; thus, the sulfide-based pollutant was effectively eliminated, and the original mineral components of the stone were largely preserved. Materials B and C had moderate changes in composition, so their desalination performance was relatively lower but

still reasonable. Material D had a small change in elemental composition and was therefore the least effective for desalination among the materials tested.

Comparing Materials E, F, G and H, Material E showed the most pronounced reduction in surface contamination after desalination and was thus relatively cleaner on the stone surface. Of all the materials that were tested, Material E showed a significant decrease in SO_3 content, at only 0.005 wt.%, and thus was suitable for removing sulfide-based pollutants. CaO and SiO_2 also increased to a certain extent; therefore, the desalt process removed water-soluble salts and other impurities, causing a relative increase in the proportions of main rock minerals. Materials F and G also reduced the concentration of surface pollutants and SO_3 to some extent, but the change in CaO and SiO_2 was relatively small. Among the two materials, Material G showed a more significant change in composition after desalination than Material F and was thus relatively more desalinating. Material H had little change in the composition of the surface.

Based on the comparison of the changes in the main components of the stone after desalination using both rice paper and pulp, it can be concluded that materials with modifiers had a much better desalting and cleaning effect than the control group. Material A reduced the SO_3 and other pollutants significantly, and increased the amount of CaO and SiO_2 after desalination. Material E also showed the largest reduction in pollutants and SO_3, and had a relatively large increase in CaO and SiO_2, indicating high efficiency for the removal of soluble salts. Desalination reduced SO_3, MgO and Fe_2O_3 effectively, and at the same time raised the relative proportion of CaO; thus, the elimination of soluble salts and secondary mineral deposits increased the concentration of primary mineral components in the stone. Importantly, no new substances, oxides or crystalline phases were found on the stone after desalination; therefore, it can be confirmed that the treatment did not damage the structure of the stone. Based on the above results, it can be concluded that sulfides and other impurities were released and thus reduced the purity of CaO in the stone matrix.

In short, based on the above results, it can be concluded that desalting pulp can enhance the desalination rate significantly when used in conjunction with a 1:2 PAA-PESA ratio, thus improving the overall performance of the desalination system.

3.5 XRD

According to the experimental results, Material E was the best for desalting. Therefore, X-ray diffraction (XRD) analysis of the composition was carried out to study alterations in the mineralogy of the stone before and after desalination.

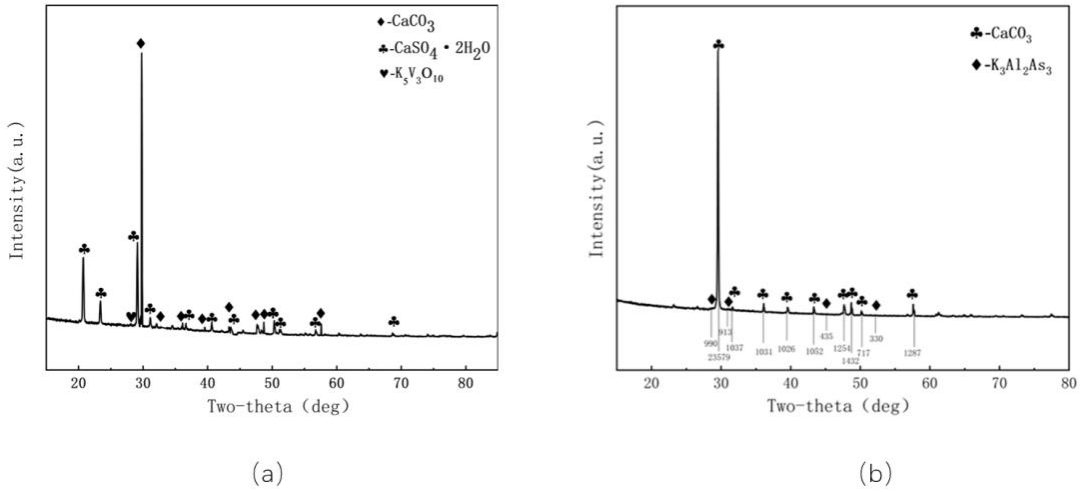

Figure 7: XRD analysis of major elemental components before and after desalination

Figure 7(a) shows the XRD results before desalination and the diffraction pattern of the stone sample powder. Multiple diffraction peaks were observed in the analysis, and the peak corresponding to $CaSO_4$ was the most frequent but had the smallest peak area. Therefore, it can be seen that although $CaSO_4$ is present in large quantities, its distribution is relatively even, and the stone has a relatively high concentration of SO_4^{2-} salts. The presence of SO_4^{2-} salts shows that the stone has been damaged by severe salt weathering over a long time. In addition, the first peak for $CaCO_3$ was the strongest and had the largest peak area; thus, it was confirmed that $CaCO_3$ was the principal mineral in the rock. A small peak for $K_5V_3O_{10}$ was also observed at the top of the rock.

Figure 7(b) is the XRD pattern of the stone sample powder after desalination, and there have been significant changes in mineral composition compared with the pre-desalination state. The diffraction pattern shows a decrease in the number of diffraction peaks; thus, it is inferred that secondary mineral phases and salt-related crystalline deposits have been reduced during desalination, and soluble salts and impurities have been removed. The peak of $CaCO_3$ is relatively high in intensity and has a larger area; therefore, it can be confirmed that the main mineral in the stone is $CaCO_3$. In addition, after desalination, a $K_3Al_2As_3$ peak has been observed on the stone surface and is thought to be a result of increased visibility after desalination.

Na_2SO_4 and $CaSO_4$ completely dissociate in the aqueous solution during desalination to produce Na^+, Ca^{2+} and SO_4^{2-}. Simultaneously, PAA and PESA are deprotonated to produce -COO^- ions that contain oxygen atoms with lone pairs of electrons. Both Na^+ and Ca^{2+} are electron-deficient and can coordinate with the oxygen lone pairs of -COOH. Cooperative interaction leads to a new molecular structure formed by PAA-PESA and Na_2SO_4, and thus modifies the crystallization process of both Na_2SO_4 and $CaSO_4$. The above molecular mechanism shows that PAA-PESA modifiers can improve the performance of salt extraction and increase the efficiency of desalination, thus promoting the long-term protection of salt-weathered stone surfaces.

In short, the XRD data before and after desalination show that no new substances, oxides or crystalline phases have been formed in the stone as a result of the treatment. Therefore, it can be concluded that the structure and chemical composition of the stone matrix have not been significantly altered during the desalination process. The above data also show that $CaSO_4$ has been effectively removed, and all the SO_4^{2-} ions in the rock have been extracted. The first kind of stone is $CaCO_3$ and is also a natural mineral. The largest peak area for $CaCO_3$ after desalination also confirms that it is the main mineral component, and thus the treatment has successfully preserved the original mineral structure of the stone. Based on the above data, it can be seen that when desalting pulp is used as the base material in combination with a 1:2 PAA-PESA solution, significantly more desalination can be achieved; at the same time, the structure of the stone will be preserved.

4 Conclusion

Three different composite modifier ratios (1:2, 1:2.5 and 1:3) were selected in this study for evaluation of the desalination efficiency of HWB rock. Based on the above experiments, adding the composite modifier to the base material effectively increased the removal rate of soluble salts; at a ratio of 1:2, this desalting performance was highest. The modifier did not change the mineral composition or microstructures of HWB rock significantly, so it was confirmed to be non-destructive. Rice paper and desalination pulp are traditional desalination materials; desalting materials containing a composite modifier have shown a significant improvement in both desalination rate and overall performance compared with the former.

By using the above methods of ion chromatography, XRD, XRF, conductivity measurement and digital microscopy, it was confirmed that the 1:2 composite modifier was superior for desalination. By the seventh day, desalinisation had been achieved, and the maximum conductivity reached 244 μS/cm; salt extraction was proceeding normally. Desalination was performed to reduce both the amount of surface and internal impurities, and the concentration of sulphides and salts in the stone was significantly reduced. High desalting capacity; it has a good effect and a fast rate of reaction, so this material is highly efficient and effective. In addition, a 1:2 composite modifier was added to improve the dissolution and separation of salts from the stone, reduce desalination time and cost, and thus address the problems of incomplete desalination and multiple treatments that occurred under the old way of desalination.

In addition, according to the experiment, after desalination with the 1:2 composite modifier, there are no residual substances on the stone surface, and therefore no secondary damage due to residue accumulation. This result has a good practical effect on the preservation of cultural heritage, can increase the efficiency of restoration, reduce conservation costs, and thus promote economically and environmentally friendly desalination.

In short, by adding a 1:2 ratio of the composite modifier to the desalting pulp for HWB desalination, it has achieved a higher desalination rate, excellent desalting performance, and rapid salt removal. A ratio of 1:2 for PAA-PESA composite modifier in desalination was employed, and at the same time, reduced both desalination time by 46% and material cost by 31.5%. This method has shown very good desalination results and is also economically feasible; thus, a new and scientifically reliable way has been found for preserving and protecting salt-weathered stone cultural relics.

References

[1] Barbara Lubelli, Rob P.J. van Hees, Effectiveness of crystallization inhibitors in preventing salt damage in building materials, Journal of Cultural Heritage, Volume 8, Issue 3, 2007, Pages 223-234, ISSN 1296-2074,

[2] Michael Steiger, Sönke Asmussen, Crystallization of sodium sulfate phases in porous materials: The phase diagram Na2SO4–H2O and the generation of stress, Geochimica et Cosmochimica Acta, Volume 72, Issue 17, 2008, Pages 4291-4306, ISSN 0016-7037,

[3] Bracciale, Maria Paola, Svetlana Sammut, JoAnn Cassar, Maria Laura Santarelli, and Assunta Marrocchi. 2020. "Molecular Crystallization Inhibitors for Salt Damage Control in Porous Materials

[4] Charles Selwitz, Eric Doehne, The evaluation of crystallization modifiers for controlling salt damage to limestone, Journal of Cultural Heritage, Volume 3, Issue 3, 2002, Pages 205-216, ISSN 1296-2074,

[5] Encarnación Ruiz-Agudo, Aurelia Ibañez-Velasco, Cristina Ruiz-Agudo, Sarah Bonilla-Correa, Kerstin Elert, Carlos Rodríguez-Navarro, Damage of porous building stone by sodium carbonate crystallization and the effect of crystallization modifiers, Construction and Building Materials, Volume 411, 2024, 134591, ISSN 0950-0618,

[6] Robert J. Flatt, Salt damage in porous materials: how high supersaturations are generated,

[7] Wen, Yaping, Huoliang Qing, Hui Shu, and Qiang Liu. 2021. "Evaluating the Protective Effects of Calcium Carbonate Coating on Sandstone Cultural Heritage" Coatings 11, no.

12: 1534.

[8] Comite, Valeria, Andrea Bergomi, Chiara Andrea Lombardi, Mattia Borelli, and Paola Fermo. 2023. "Characterization of Soluble Salts on the Frescoes by Saturnino Gatti in the Church of San Panfilo in Villagrande di Tornimparte (L'Aquila)" Applied Sciences 13, no. 11: 6623.

[9] Journal of Crystal Growth, Volume 242, Issues 3–4, 2002, Pages 435-454, ISSN 0022-0248,

[10] Dei L, Mauro M, Baglioni P, Growth of Crystal Phases in Porous Media. Langmuir, 1999, 15 (26)8915~8922.

[11] D. Benavente, M.A.Garcı́a del Cura, J. Garcı́a-Guinea, S. Sánchez-Moral, S. Ordóñez, Role of pore structure in salt crystallisation in unsaturated porous stone, Journal of Crystal Growth, Volume 260, Issues 3–4, 2004, Pages 532-544, ISSN 0022-0248,

[12] Chen, Wen, wuChen, HaoxinJia, BoboBi, JunLi, Xiang Study of salt migration on the upper part of the Great Wall under the rainfall-radiation cycle20222022/09/15

[13] Tounsi, Hafssa Rutqvist, Jonny, Hu, Mengsu, Kuhlman, Kristopher Thermo-Hydro-Mechanical Modeling of Brine Migration in a Heated Borehole Test in Bedded Salt Rock Mechanics and Rock Engineering2024, 2024/08/01

[14] E. Bresler, Transport of salts in soils and subsoils, Agricultural Water Management, Volume 4, Issues 1–3, 1981, Pages 35-62,

[15] Blen Taye, Heather Viles, Hong Zhang, Influence of salt (NaCl) on hydric and hygric dilatation of clay-rich rocks, Journal of Cultural Heritage, Volume 58, 2022, Pages 137-145, ISSN 1296-2074

[16] Jing Zhao, Hongjie Luo, Transport and crystallization of NaCl solution in porous silicate materials, Journal of Crystal Growth, Volume 519, 2019, Pages 25-34, ISSN 0022-0248,

[17] Xin Liu, Xilin Shi, Yinping Li, Liangliang Ye, Xinxing Wei, Shijie Zhu, Weizheng Bai, Hongling Ma, Chunhe Yang, Synthetic salt rock prepared by molten salt crystallization and its physical and mechanical properties, Energy, Volume 269, 2023, 126711, ISSN 0360-5442,

[18] [Encaracio'n Ruiz-Agudo, Carlos Rodriguez-Navaro, Eduardo Sebastia'n-Pardo, Sodium Sulfate Crystallization in the Presence of Phosphonates Implications in Omamental Stone Conservation.CRYSTAL GROWTH & DESIGN 2006., 6(7):1575-1583

[19] Mitigating salt damage in building materials by the use of crystallization modifiers – a review and outlook, Journal of Cultural Heritage, Volume 40, 2019, Pages 183-194, ISSN 1296-2074,

[20] Nadine Lindström, Nicole Heitmann, Kirsten Linnow, Michael Steiger, Crystallization behavior of NaNO3–Na2SO4 salt mixtures in sandstone and comparison to single salt behavior, AppliedGeochemistry, Volume 63, 2015, Pages 116-132, ISSN 0883-2927,

[21] Christopher Hall, Andrea Hamilton, The heptahydrate of sodium sulfate: Does it have a role in terrestrial and planetary geochemistry?, Icarus, Volume 198, Issue 1, 2008, Pages 277-279, ISSN 0019-1035,

[22] A.I. Vavouraki, P.G. Koutsoukos, The inhibition of crystal growth of mirabilite in aqueous solutions in the presence of phosphonates, Journal of Crystal Growth, Volume 436, 2016, Pages 92-98, ISSN 0022-0248,

[23] Carlos Rodriguez-Navarro, Eric Doehne, Eduardo Sebastian, How does sodium sulfate crystallize? Implications for the decay and testing of building materials, Cement and Concrete Research, Volume 30, Issue 10, 2000, Pages 1527-1534, ISSN 0008-8846,

[24] Hannelore Derluyn, Tamerlan A. Saidov, Rosa M. Espinosa-Marzal, Leo Pel, George W. Scherer, Sodium sulfate heptahydrate I: The growth of single crystals, Journal of Crystal Growth, Volume 329, Issue 1, 2011, Pages 44-51, ISSN 0022-0248,

[25] Dalia Bednarska, Marcin Koniorczyk, Michael Steiger, Identification of various salt crystallization and water freezing patterns induced by temperature variation from Na2SO4 – H2O system confined in porous materials, Construction and Building Materials, Volume 347, 2022, 128540, ISSN 0950-0618,

[26] Tamerlan A. Saidov, Rosa M. Espinosa-Marzal, Leo Pel, George W. Scherer, Nucleation of sodium sulfate heptahydrate on mineral substrates studied by nuclear magnetic resonance,

[27] E. Bresler, Transport of salts in soils and subsoils, Agricultural Water Management, Volume 4, Issues 1–3, 1981, Pages 35-62,

[28] Yu S, Oguchi C T. Complex relationships between salt type and rock properties in a durability experiment of multiple salt-rock treatments, Earth Surf.Process, Landforms. 2009, 34 (15):2096~2110.

[29] Ruiz Agudo E, Mees F, Jacobs P, Rodriguez Navaro C. The role of saline solution properties onporous limestone salt weathering by magnesium and sodium sulfates. Environ. Geol., 2007, 52 (2):269~281.

[30] Rodriguez Navarro C, Doehne E. Salt weathering: influence of evaporation rate, supersaturation andcrystallization pattern. Earth Surf. Process. Landf, 1999, 24 (3): 191~209.

[31] Liu, R., Zhang, B., Wei, G., et al. (2016). Investigation on pollution-related diseases in the Yungang Grottoes. Sciences of Conservation and Archaeology, 28(2), 103-104.

[32] Jie Li, Dandan Liu, Hongkun Jiang, Jun Wang, Xiaoyan Jing, Rongrong Chen, Wenting Zhu, Shihui Han, Wanyou Li, Hao Wei, Effects of polyacrylic acid additive on barium sulfate particle morphology, Materials Chemistry and Physics, Volume 175, 2016, Pages 180-187, ISSN 0254-0584,

[33] Jay Thakkar, Sai Bhargav Annavajjala, Jan Kosny, Margaret J. Sobkowicz, Stabilizing a low temperature phase change material based on Glaubers salt, Journal of Energy Storage, Volume 91, 2024, 111936, ISSN 2352-152X,

[34] Dong-Mei Chen, Kun Yuan, Xian-Ming Zhang, Morphology transformation of Na2SO4 from prism into dendrite enhanced desalination efficiency in sandstone by biodegradable polycarboxylate modifiers, Construction and Building Materials, Volume 411, 2024, 134513, ISSN 0950-0618,

[35] Sanne J.C. Granneman, Barbara Lubelli, Rob P.J. van Hees, Effect of mixed in crystallization modifiers on the resistance of lime mortar against NaCl and Na2SO4 crystallization, Construction and Building Materials, Volume 194, 2019, Pages 62-70, ISSN 0950-0618,

[36] Mohsen M. Saleh, Sawsan S. Darwish, M. Elzoghby, The effectiveness of some crystallization inhibitors in preventing salt damage to limestone, Journal of Crystal Growth, Volume 585, 2022,

[37] Chen, D., & Zhao, S. (2023). A study on desalination using a compound modifier in grotto rock mass. Chongqing Architecture, (7), 42-45.